Scientia Iranica A (2019) 26(1), 188–201

Sharif University of Technology
Scientia Iranica
Transactions A: Civil Engineering
http://scientiairanica.sharif.edu

Near-fault effects on the seismic demand of RC buildings in linear and nonlinear analyses

M.H. Mohammadi, A. Massumi*, and A. Meshkat-Dini

Department of Civil Engineering, Faculty of Engineering, Kharazmi University, No. 43, Dr. Mofatteh Ave., Tehran, 15719-14911, Iran.

Received 15 January 2017; received in revised form 16 May 2017; accepted 15 July 2017

KEYWORDS
Near-fault ground motion;
Seismic demand;
Linear response history analysis;
Nonlinear response history analysis;
Ductility.

Abstract. Strong ground motions of near-fault earthquakes are mostly generated by forward-directivity effects. Forward-directivity effects develop energetic pulses, particularly in the horizontal velocity history of the fault-normal component. The narrow-band nature of the pulses results in the occurrence of at least two peaks on the response spectra as well as increase in seismic demand, especially in mid-rise and high-rise buildings. Iranian seismic code (IS 2800-14) presents the coefficient N for considering near-fault effects. It seems that N is not efficient for designing in near-fault zone. The accurate near-fault demands can be determined by using nonlinear response history analyses. In the present paper, two 3-D reinforced concrete framed structures (RC buildings) are designed according to ACI 2014 and IS 2800-14. Then, the demands are estimated by employing Linear Response History Analysis (LRHA) and Nonlinear Response History Analysis (NRHA) under an ensemble of 11 near-fault ground motions. The results reveal that the design spectrum of IS 2800-14 is incompatible with near-fault spectra and underestimates demands in the long periods range. Further, implementation of LRHA using response modification factor (R_u) and deflection amplification factor (C_d) leads to insufficient inter-story drift ratios. Finally, the influence of enhancing ductility is studied by determining ductility reduction factors for near-fault records.

1. Introduction

Earthquakes such as Parkfield 1966 in California and Pacoima Dam 1971 in San Fernando can be considered as the first significant near-fault ground motions during the last decades. The occurrence of catastrophic earthquakes such as Landers 1992, Northridge 1994, Kobe 1995, and Chi-Chi 1999 in the 1990s led researchers to investigate the near-fault effects on structural designing [1]. Propagation of fault rupture with a velocity close to the shear wave velocity toward the site generates forward-directivity effects and accumulation of seismic radiations results in developing a long-period and high-amplitude pulse in the beginning of the velocity history. Due to the inclination of shear waves' accumulation toward the normal direction of rupture, the fault-normal components are stronger than the fault-parallel ones [2]. In 1975, the pulses of near-fault records were distinguished for the first time [3]. If the site is located behind the rupture direction, backward-directivity will occur and the records may have low amplitudes and short durations.

Seismic demands are widely concerned with the ratio of the velocity pulse period to the fundamental period ($T_{\text{pulse}}/T_{\text{structure}}$) and the ratio of the PGA to

*. *Corresponding author. Tel.: +98 21 88830891; Fax: +98 21 88329213;*
E-mail addresses: std_h.mohammadi@khu.ac.ir (M.H. Mohammadi); massumi@khu.ac.ir (A. Massumi); Meshkat@khu.ac.ir (A. Meshkat-Dini)

doi: 10.24200/sci.2017.4233

the lateral stiffness. Generally, high deflections in lower stories increase axial forces of columns and $P-\Delta$ effects in lower stories [4]. Fling step in the direction parallel to faulting appears like a static displacement and typically excites the first mode of structural vibration [5]. Alavi and Krawinkler [2] recognized the high seismic demands of structures in the direction of the fault-normal component. They also claimed that the spectral analysis yielded inappropriate results. The excitation of higher modes in high-rise buildings, due to wave travelling effect, leads to premature yield. Consequently, the upper stories quickly reach their shear capacity. Chang and Yu [6] modified the design spectrum of Taiwan in the long periods range, comparing Chi-Chi records with ordinary records. Choi et al. [7] studied the design spectrum of nuclear site in Korea and recognized the incompatibility of this spectrum with the near-fault spectrum at low frequencies. Choi et al. [8] stated the inadequacy of Caltrans 1.3 spectrum at long periods and its overestimation at short periods after studying the near-fault effect on bridge columns designed according to Caltrans. Su et al. [9] compared the design spectrum of American electrical equipment with the spectrum obtained from Chi-Chi accelerograms in different soil types and then, pointed out that the design spectrum should have larger values at low frequencies due to the forward-directivity effects and the amplification of soft soils. Hatzigeorgiou [10] quantified the seismic sequence effect directly on ductility demand spectra under multiple near- and far-fault seismic ground motions and showed that near-fault and far-fault earthquakes required different ductility demands, not only for single earthquakes but also for multiple ones. Durucan and Durucan [11] developed some equations to express the inelastic displacement ratio for estimating the seismic response of structures subjected to sequential near-fault ground motions. Yaghmaei-Sabegh and Tsang [12] concentrated on the ground motions of the 1978 Tabas and proposed a combined method for simulating the impulsive nature of the Tabas earthquake.

Champion and Liel [13] comprehensively researched on the $T_{\text{pulse}}/T_{\text{structure}}$ and declared that structures which were designed to be elastic experienced the highest demand when $T_{\text{pulse}}/T_{\text{structure}}$ equaled 1. Whereas, ductile structures underwent the highest demand in $T_{\text{pulse}}/T_{\text{structure}}$ close to 2, due to the elongation of the period before collapse. Their study also demonstrated the importance of considering directivity effects in seismic hazard analysis and simulation of structural response. For instance, as the pulse-type effects of ground motions were not considered in fragility curves, the collapse probability in 50 years was underestimated close to 50%. Many researches on strengthening of moment resisting frames [14-16] and different procedures through base isolation [17-19] or energy dissipation systems [20-23] have been carried out for improving the seismic performance. Gerami and Abdollahzadeh [24] studied the Iranian design spectrum of IS 2800-05 and showed that spectral acceleration values of records having forward-directivity effects were at least two times the corresponding values of IS 2800-05 at periods longer than 1 s.

So many buildings are founded near active faults in Iran. Newly, IS 2800-14 has been revised to consider the near-fault effect on the design spectrum for periods longer than the soil period by defining the coefficient N. It should be noted that the coefficient N is not able to apply the directivity effects in seismic design efficiently. It could be helpful to implement NRHA as well as LRHA for assessing the performance of buildings designed according to IS 2800-14. Hence, in this study, base shears and inter-story drift ratios of two reinforced concrete buildings with five and ten stories are compared using LRHA and NRHA under near-fault earthquakes.

2. Structural specifications and response history analyses

2.1. Structural models

Two regular 3-D reinforced concrete moment frame buildings including 5 and 10 stories, erected on the soil type 2 ($\bar{v}_s = 375 - 750$ m/s), are analyzed linearly and designed according to ACI 2014 code [25]. The seismic loading and analysis are based on Iranian seismic code (IS 2800-14) [26]. IS 2800 is considerably similar to ASCE 7 (ASCE/SEI) [27]. The compressive strength and Young modulus of concrete are assumed 25 MPa and 26 GPa, respectively. Yield strength and Young modulus of reinforcement steel are also assumed 400 MPa and 200 GPa, respectively. Plan and elevations of the buildings can be seen in Figure 1, and dimensions of the structural components are shown in Tables 1 and 2.

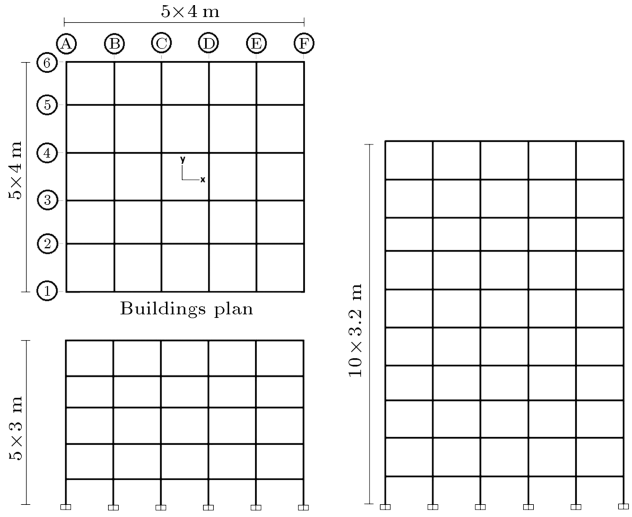

Figure 1. Plan and elevations of studied buildings.

Table 1. Structural details of the 5-story building.

	Beams		Columns	
Story	$b \times h$ **(no.-bar size)**	A_v/S	$b \times h$ **(no.-bar size)**	A_v/S
1	45 × 45 (4-20 d)	0.1	50 × 50 (20-20 d)	0.157
2	45 × 45 (4-20 d)	0.1	50 × 50 (20-20 d)	0.157
3	40 × 40 (4-20 d)	0.1	45 × 45 (16-18 d)	0.157
4	40 × 40 (4-18 d)	0.1	45 × 45 (16-18 d)	0.157
5	40 × 40 (4-18 d)	0.1	45 × 45 (12-18 d)	0.157

Note: Dimensions are in centimeter.

Table 2. Structural details of the 10-story building.

	Beams		Columns	
Story	$b \times h$ **(no.-bar size)**	A_v/S	$b \times h$ **(no.-bar size)**	A_v/S
1	50 × 50 (4-20 d)	0.157	55 × 55 (20-20 d)	0.157
2	50 × 50 (5-20 d)	0.157	55 × 55 (20-20 d)	0.157
3	45 × 45 (5-20 d)	0.157	50 × 50 (16-20 d)	0.157
4	45 × 45 (5-20 d)	0.157	50 × 50 (16-20 d)	0.157
5	45 × 45 (5-20 d)	0.157	50 × 50 (16-20 d)	0.157
6	45 × 45 (6-18 d)	0.157	50 × 50 (16-20 d)	0.157
7	40 × 40 (5-18 d)	0.157	50 × 50 (16-18 d)	0.157
8	40 × 40 (5-18 d)	0.157	50 × 50 (16-18 d)	0.157
9	40 × 40 (5-18 d)	0.157	50 × 50 (16-18 d)	0.157
10	40 × 40 (5-18 d)	0.157	50 × 50 (16-18 d)	0.157

Note: Dimensions are in centimeter.

Table 3. Modal analysis results of the first nine modes.

Mode no.	**Name**	**5-Story building**		**10-Story building**	
		Period (sec)	**MEMR*** **(%)**	**Period (sec)**	**MEMR (%)**
1	T_{1X}	0.660	73.7	1.071	75.2
2	T_{1Y}	0.660	73.7	1.071	75.2
3	$T_{1\theta}$	0.602	76.6	0.972	75.8
4	T_{2X}	0.217	8.5	0.376	10.8
5	T_{2Y}	0.217	8.5	0.376	10.8
6	$T_{2\theta}$	0.199	14.0	0.344	11.5
7	T_{3X}	0.114	4.2	0.214	5.4
8	T_{3Y}	0.114	4.2	0.214	5.4
9	$T_{3\theta}$	0.106	5.0	0.198	5.6

*MEMR: Modal Effective Mass Ratio

Dead and live loads are considered 5.5 kN/m^2 and 2 kN/m^2 for typical stories and 6 kN/m^2 and 1.5 kN/m^2 for roof, respectively. Equivalent dead loads of circumferential walls and interior partition walls are considered 2 kN/m^2 and 1.5 kN/m^2. Seismic mass includes 100% of the dead load and 20% of the live load for residential buildings. Modal analysis results are shown in Table 3. In order to design buildings, Spectral Analysis (SA) is implemented and the response modification factor (response reduction factor) $R_u = 5$ is applied. Due to the destructive manner of near-fault earthquakes, the strong column and weak beam rule is absolutely observed in the seismic design. Near-fault effects are considered in the design spectrum of IS 2800-14 by means of the N coefficient. For sites with high seismicity, N is

expressed by Eq. (1) in the period range of the soil period (T_s) to 4 s.

$$N = \frac{0.7}{4 - T_s}(T - T_s) + 1. \quad (1)$$

2.2. Selecting and scaling of records

Selected accelerograms must be scaled for response history analyses. In addition to the earthquake characteristics and the site effects, the spectral shape over the period range of 0.2 T_1 to 1.5 T_1 is an extremely important issue for scaling the far-fault records to a target spectrum in ASCE/SEI 7 and IS 2800-14. However, the existence of velocity pulses as well as the spectral shape must be considered for scaling the near-fault records. If the spectral shapes of the pairs of the accelerograms are similar to the target (design) spectrum, the need for scaling and modifications will be decreased [28]. Velocity pulses are present in many ground motions, especially in the forward-directivity region. In this study, fault-parallel and fault-normal components of 11 strong earthquakes, with magnitudes of over 6.5, are selected from PEER Ground Motion Database. Table 4 provides characteristics of the selected ensemble. Some of the velocity pulses are shown in Figure 2. The fault-parallel or longitudinal component (LN) and fault-normal or transversal component (TR) are applied in the structural directions of X and Y, respectively.

The ELC earthquake with a hypocentral distance of 12.2 km contains no directivity effects and is con-

Table 4. Characteristics of the selected ensemble.

No.	Event	Station	Rrup (km)	Component ID	SD* (sec)	SED* (cm^2/s)	T_{pulse}* (sec)
1	Imperial valley-02	El Centro array #9	6.09	ELC-LN	23.63	1940.19	–
				ELC-TR	23.84	1548.27	–
2	Manjil, Iran	Abbar	12.55	ABR-LN	10.76	2001.93	–
				ABR-TR	20.02	4963.60	2.00
3	Northridge-01 1994	LA-Sepulveda VA-hospital	8.44	SPV-LN	8.26	4513.93	0.60
				SPV-TR	7.86	4039.00	1.00
4	Northridge-01 1994	Newhall-W Pico Canyon Rd.	5.48	WPI-LN	10.91	3698.21	0.80
				WPI-TR	6.97	9402.91	2.00
5	Erzican, Turkey	Erzincan	4.38	ERZ-LN	11.80	4512.01	1.00
				ERZ-TR	15.31	7080.23	3.00
6	Bam, Iran	Bam	1.70	BAM-LN	8.70	3033.55	1.60
				BAM-TR	7.77	7992.26	1.50
7	Tabas, Iran	Tabas	2.05	TAB-LN	16.36	14145.95	0.75
				TAB-TR	16.10	34006.88	6.20
8	Imperial valley-06	El Centro array #6	1.35	E06-LN	11.42	4779.72	2.00
				E06-TR	8.24	14672.31	3.70
9	Imperial valley-06	El Centro array #7	0.56	E07-LN	6.75	3172.38	1.50
				E07-TR	4.80	10196.47	3.00
10	Landers	Lucern	2.19	LCN-LN	13.78	1504.81	–
				LCN-TR	13.50	20075.91	4.80
11	Landers	Joshua Tree	11.03	JOS-LN	26.94	1964.23	–
				JOS-TR	25.98	3726.62	–

*SD, SED, and T_{pulse} denote significant duration, specific energy density, and velocity pulse period, respectively.

Table 5. Scale factors obtained based on IS 2800-14 for NRHA.

Record	5-Story building			10-Story building		
	Single	Average	Finally applied	Single	Average	Finally applied
ELC	1.41	1.47	1.41	1.65	1.47	1.65
ABR	0.97	0.89	1.00	1.33	0.89	1.33
SPV	0.61	0.49	1.00	0.88	0.49	1.00
WPI	1.57	1.01	1.57	1.20	1.01	1.20
ERZ	0.98	0.89	1.00	0.97	0.89	1.00
BAM	0.88	0.58	1.00	0.88	0.58	1.00
TAB	0.52	0.54	1.00	0.62	0.54	1.00
E06	1.26	1.04	1.26	1.20	1.05	1.20
E07	1.05	0.99	1.00	1.10	0.99	1.00
LCN	1.60	0.58	1.60	1.60	0.58	1.60
JOS	2.08	1.62	2.08	1.47	1.62	1.47

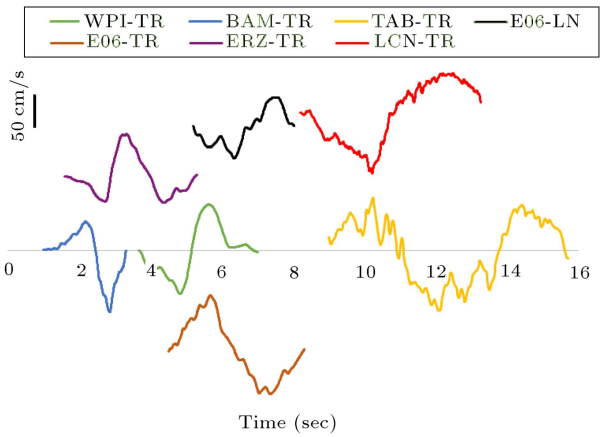

Figure 2. Some of the existing pulses in the velocity history of records.

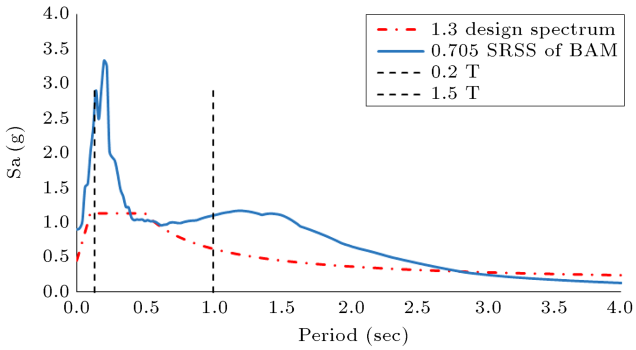

Figure 3. The difference between scaled spectrum of BAM and the design spectrum (5-story).

sidered as a strong far-fault earthquake. Other earthquakes are near-fault with forward-directivity effects, except for JOS, which involves backward-directivity effects. It is worth noting here that the stronger near-fault ground motions such as TAB-TR and LCN-TR containing high energetic pulses have large values of Specific Energy Densities (SED), as shown previously in Table 4. SED is defined by Eq. (2), where v is the velocity of the ground motions.

$$SED = \int_0^{t_{tot}} v^2 dt. \tag{2}$$

Scaling method on the basis of IS 2800-14 is analogous to ASCE/SEI 7-10. Accordingly, the SRSS of normalized spectra of horizontal components is compared with 1.3 times the design spectrum in the range of 0.2 T_1 to 1.5 T_1, where T_1 is the first mode translational period. Iranian design spectrum is obtained with a probability of exceedance of 10% in 50 years (design-basis earthquake, DBE), and it advises seismic acceleration coefficient $A = 0.35$ g for the zone exposed to high level of hazard. The scale factors of records are once obtained by comparing the SRSS of the spectra of a single earthquake (single scaling method) and the next time, by comparing the average of the SRSSs of the spectra of 11 earthquakes (average scaling method) with 1.3 times the design spectrum, as reported in Table 5.

The values in the third column of Table 5 are used as the suitable scale factors for the NRHA. It is obvious that the scale factors of LRHA can be attained by dividing the NRHA scale factors by the response modification factor ($R_u = 5$). Some scale factors are obtained smaller than 1 and should not be used, in order to avoid the attenuation of the free-field records. Thus, scale factors smaller than 1 are considered equal to 1. Figures 3 and 4 illustrate two instances of the difference between scaled SRSS spectrum and 1.3 times the design spectrum, especially in periods longer than 1 s. The differences are related to the high

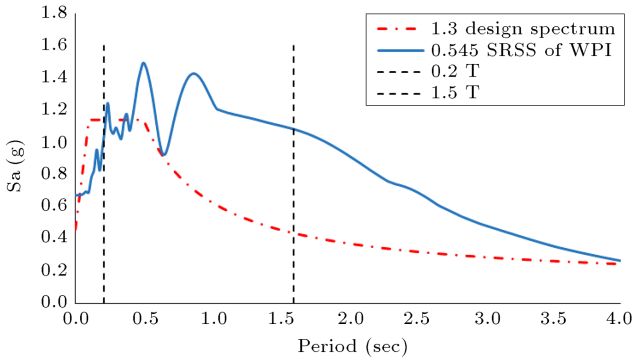

Figure 4. The difference between scaled spectrum of WPI and the design spectrum (10-story).

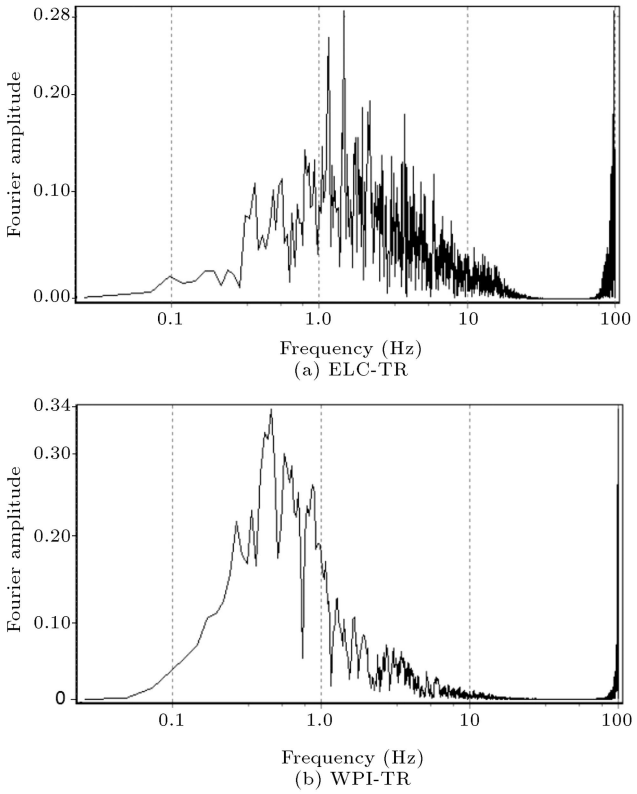

Figure 5. Fourier amplitude spectra of (a) a far-fault (ELC-TR) and (b) a near-fault record (WPI-TR).

amplitudes of near-fault Fourier Spectra at frequencies lower than 1 Hz, as shown in Figure 5. As well, it seems that the single scaling is more appropriate than the average scaling. Average scaling method decreases the important peaks of near-fault spectra and yields smaller scale factors due to the smooth spectrum obtained by averaging the SRSSs, as demonstrated in Figure 6.

2.3. Modeling of components and response history analyses

In order to assess buildings by implementation of LRHA and NRHA, SAP2000 version 18.1.1 is employed. The provisions and recommendations of the

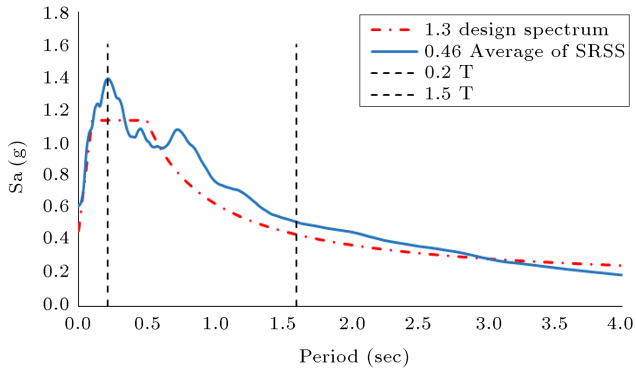

Figure 6. The average spectrum scaled with the design spectrum (10-story).

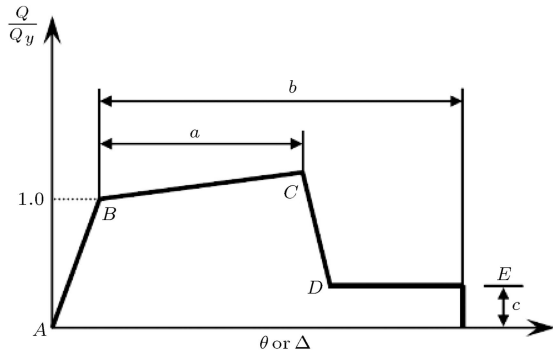

Figure 7. Generalized force-deformation relation for RC ductile components (after ASCE/SEI 41-13).

ASCE/SEI 41-13 (Seismic Evaluation and Retrofit of Existing Buildings) [29] are used for modeling of the nonlinear behavior of components, considering concentrated plastic hinges. According to ASCE 41-13, customary behavior curve of deformation-controlled members is similar to Figure 7.

The following conditions are considered in the seismic analyses and assessment:

1. Deformation-controlled hinges are located at the distances equal to the half-height of members from end rigid zones and they follow Takeda hysteresis model [30];
2. Based on the axial force value, columns may behave either in ductile manner or in brittle manner; therefore, this issue is considered in modelling according to ASCE 41-13 criteria;
3. Modal and HHT (Hilber-Hughes-Tailor) direct integration methods [31] are employed in LRHA and NRHA, respectively, considering damping ratio of 5%;
4. Connections and diaphragms are rigid and $P-\Delta$ effect is considered in both LRHA and NRHA;
5. Fault-parallel and fault-normal components of records are applied in the X and Y structural directions, respectively.

3. Results

3.1. Base shear demand

On the basis of the Spectral Analysis (SA), the 5- and 10-story buildings are designed for the base shears of 3225.1 and 4621.5 kN, respectively. The base shears obtained from LRHA and NRHA are provided in Tables 6 and 7. In addition, the performance levels of buildings are shown beside the base shears of NRHA. It is seen that the LRHA base shears are larger than the design base shear in many cases. This problem can be attributed to the insufficient design spectrum of IS 2800-14. Thus, the design base shear should be improved. On the other hand, the buildings must withstand up to their yield base shears by utilizing the overstrengths. Additionally, the performance levels must not exceed the Life Safety (LS) according to the IS 2800-14; however, the performance levels of the buildings quickly reach or exceed the Collapse Prevention (CP) under strong earthquakes based on the NRHA results. The damage patterns of the buildings will be discussed in the next section.

3.2. Inter-story drift ratio demand and damage pattern

Recent researches related to the effects of forward-directivity on stories displacement and vulnerability of structures indicate the significant influence of

Table 6. Base shears (kN) and performance levels of the 5-story building.

Earthquake	LRHA		NRHA		
	V-X	V-Y	V-X	V-Y	PL*
ELC	2547.30	2679.92	5442.50	5978.20	IO
ABR	2988.62	1666.98	6088.90	6378.60	IO
SPV	4422.50	6427.47	6701.10	7248.40	CP
WPI	2980.01	3888.15	7830.70	12469.00	CP
ERZ	4118.52	2822.72	5842.10	7154.90	LS
BAM	2935.47	3300.58	6924.90	8061.50	LS
TAB	5097.75	5232.23	6461.20	7130.60	CP
E06	3023.16	2824.82	6774.60	7710.30	LS
E07	2794.50	4290.00	7510.60	7301.50	LS
LCN	1997.10	5009.87	6125.10	10116.90	CP
JOS	5191.31	6597.15	6729.80	8502.20	CP
Average	3463.29	4067.26	6584.68	8004.74	–

*PL: Performance levels IO, LS, and CP.

Table 7. Base shears (kN) and performance levels of the 10-story building.

Earthquake	LRHA		NRHA		
	V-X	V-Y	V-X	V-Y	PL*
ELC	3757.04	5398.20	7483.77	7396.92	IO
ABR	2751.33	4627.36	8156.27	9358.58	CP
SPV	3897.99	6991.50	7012.53	10522.93	LS
WPI	5433.27	8307.32	9113.39	9182.70	CP
ERZ	4630.55	6429.11	6400.82	8805.42	CP
BAM	5261.99	7305.80	4486.57	8971.76	CP
TAB	4481.30	4971.83	7079.46	8976.93	CP
E06	5015.82	4069.95	8849.46	9328.68	CP
E07	4591.36	4237.37	8034.26	8780.60	CP
LCN	4217.81	7685.07	7783.49	11468.30	CP
JOS	5177.74	6614.36	6733.30	8079.31	IO
Average	4474.20	6057.99	7375.75	9170.19	–

*PL: Performance levels IO, LS, and CP.

$T_{\text{Pulse}}/T_{\text{Structure}}$. The larger $T_{\text{Pulse}}/T_{\text{Structure}}$, where the higher inter-story drift ratio, especially in lower stories [32]. According to ASCE 41-13 and ASCE 7, plastic hinge rotation and maximum nonlinear inter-story drift ratio are well-known as the current seismic performance indicators associated with structural components (local scale) and whole structure (global scale), respectively.

As a result of this study, the first story columns of moment frame buildings, particularly corner ones, are the most vulnerable members, which collapse abruptly under strong near-fault ground motions; however, collapses of the columns after the beams in lower stories are observed in several cases. Inter-story drift ratios obtained based on LRHA are illustrated in Figures 8 to 11. LRHA underestimates the drift ratios so that the majority of the results are lower than 0.02, while NRHA denotes CP (Collapse Prevention) performance level frequently owing to the high values of drift ratio, as illustrated in Figures 12 to 15. It is substantial to point out here that the factors R_u and C_d are used in LRHA. Since the scale factors of ground motions in LRHA are divided by response modification factor (R_u), the calculated inter-story drift ratios must be

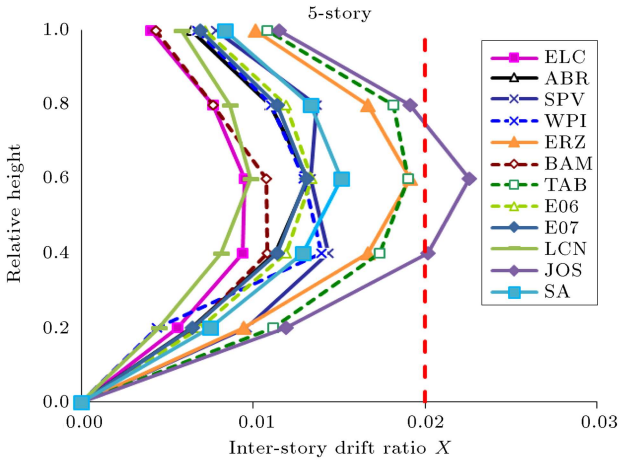

Figure 8. Inter-story drift ratios of LRHA for 5-story building (X-direction).

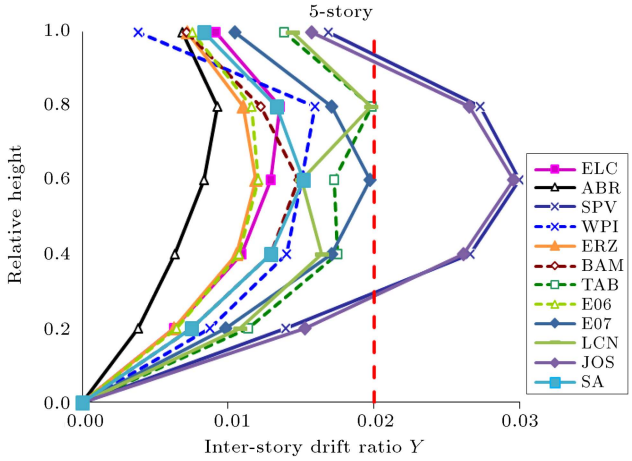

Figure 9. Inter-story drift ratios of LRHA for 5-story building (Y-direction).

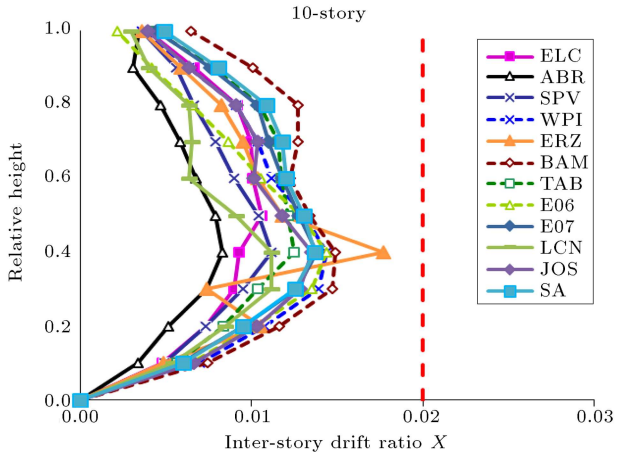

Figure 10. Inter-story drift ratios of LRHA for 10-story building (X-direction).

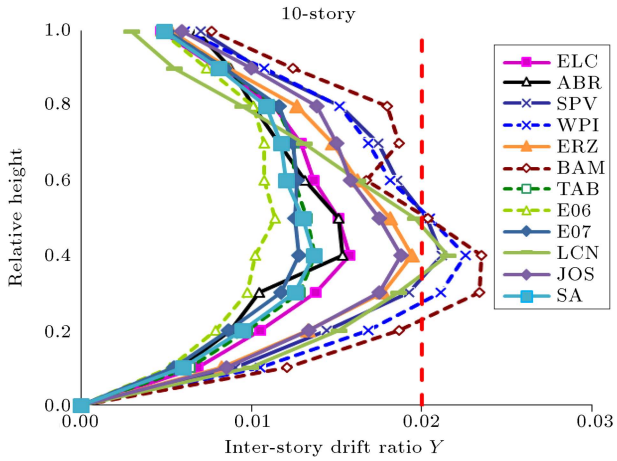

Figure 11. Inter-story drift ratios of LRHA for 10-story building (Y-direction).

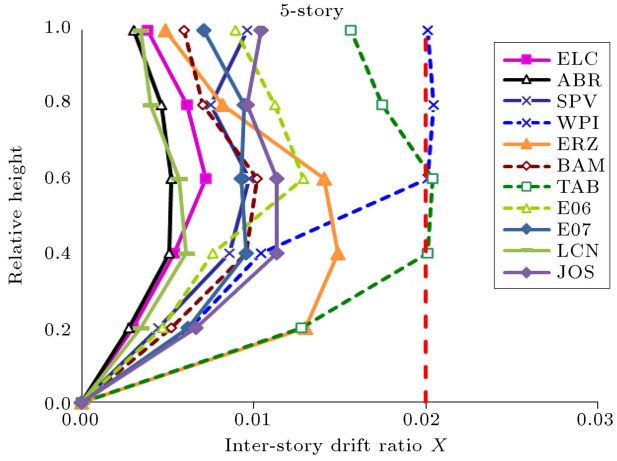

Figure 12. Inter-story drift ratios of NRHA for 5-story building (X-direction).

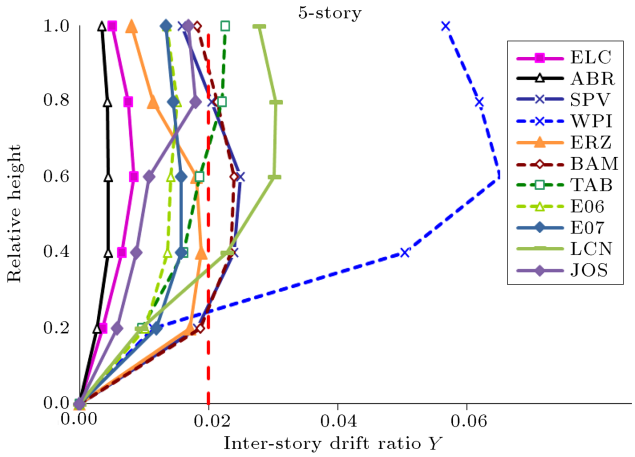

Figure 13. Inter-story drift ratios of NRHA for 5-story building (Y-direction).

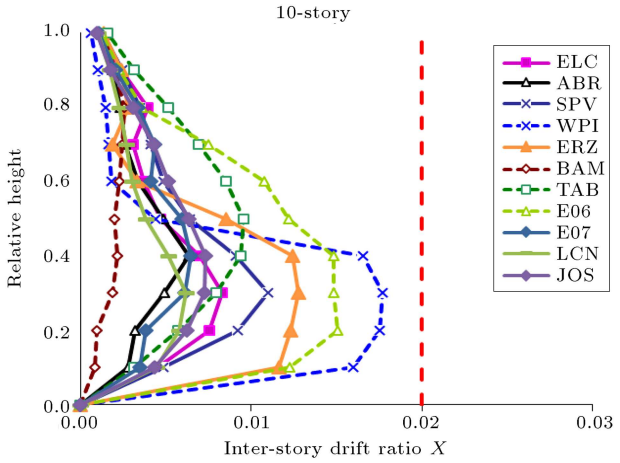

Figure 14. Inter-story drift ratios of NRHA for 10-story building (X-direction).

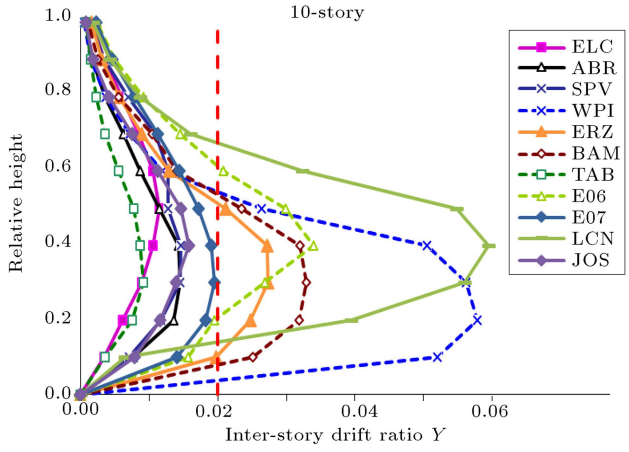

Figure 15. Inter-story drift ratios of NRHA for 10-story building (Y-direction).

multiplied by the deflection amplification factor (C_d) for determining the real inter-story drift ratios. On the basis of IS 2800-14, $C_d = 4.5$ is used for both buildings. Meanwhile, inter-story drift ratio of 0.02

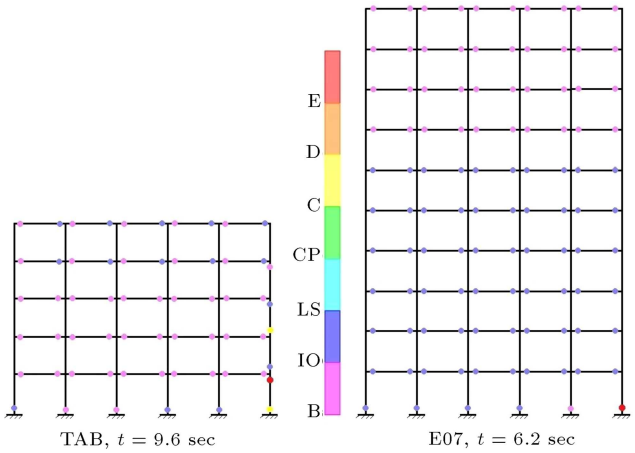

Figure 16. Collapse of the corner column in the first story under TAB and E07 records.

is the allowable value of IS 2800 and equivalent to LS (Life Safety) performance level in ASCE/SEI 7-10 as well as IS 2800-14.

It is observed that the drift ratios of the Y-direction are larger than those of the X-direction in both analyses; nevertheless the drift ratios of LRHA disagree with the drift ratios of NRHA. Implementation of LRHA by using R_u and C_d yields unacceptable results, especially for the 10-story building. It is important to point out that the diagrams of inter-story drift ratios of earthquakes such as TAB, E07, and ABR demonstrate small values, because of the abrupt collapses of the first story corner column. For better assessment of structural manner, the qualitative pattern of damage and the time of collapse are summarized in Tables 8 and 9.

As stated in Tables 8 and 9, both buildings, especially the 10-story one, collapse either at the time close to the peaks of the velocity pulses or at the ends of the pulses. Figure 16 demonstrates two samples of the first story corner columns collapses under strong near-fault ground motions. Hence, the buildings may be threatened by progressive collapse. It is substantial to note that the JOS earthquake with backward-directivity effects is similar to a narrow-band excitation. The significant duration of the transversal component of JOS is 27 s. More specifically, equality of the predominant period of the JOS-TR to the fundamental period of the 5-story building causes the dynamic resonance and collapse of the 5-story building. While, the 10-story building remains at IO performance level under the JOS earthquake.

4. Discussion

The key role of ductility in dissipating input earthquake energy considerably affects the seismic behavior of structures [33]; however, strength can become more essential according to the regions of tripartite spectra.

Table 8. Damage patterns and collapse times of the 5-story building.

Record ID	Damage pattern of the 5-story building
ELC	No structural damage occurred.
ABR	No structural damage occurred.
SPV	2nd story beams of Y-direction reached CP level at the end of the velocity pulse ($t = 3.9$ s).
WPI	2nd to 5th story beams reached CP level nearly at the end of the velocity pulse ($t = 5.8$ s).
ERZ	1st and 2nd story beams and 1st story columns reached LS level.
BAM	All beams of Y-direction and 1st story columns reached LS level.
TAB	Abruptly, one of the 1st story corner columns reached CP level at the 1st peak of the pulse ($t = 9.6$ s).
E06	All beams of Y-direction and 1st story columns reached LS level.
E07	All beams of Y-direction and 1st story columns reached LS level.
LCN	Abruptly, one of the 1st story corner columns reached CP level after the 1st peak of the pulse ($t = 10.6$ s).
JOS	Abruptly, one of the 1st story corner columns reached CP level at $t = 9.1$ s, due to dynamic resonance.

Table 9. Damage patterns and collapse times of the 10-story building.

Record ID	Damage pattern of the 10-story building
ELC	No structural damage occurred.
ABR	Abruptly, one of the 1st story corner columns reached CP level at the end of the velocity pulse ($t = 11.9$ s).
SPV	2nd to 6th story beams of Y-direction reached LS level.
WPI	1st to 3rd story beams reached CP level at the half of the velocity pulse ($t = 5.2$ s).
ERZ	1st to 3rd story beams and a corner column of the 1st story reached CP level at the peak of pulse ($t = 3.4$ s).
BAM	1st to 4th story beams reached CP level at the same time in the end of velocity pulse ($t = 3.3$ s).
TAB	Abruptly, one of the 1st story corner columns reached CP level after the 1st peak of the pulse ($t = 10.9$ s).
E06	2nd to 5th story beams of Y-direction reached CP level nearly after the half of velocity pulse ($t = 7$ s).
E07	Abruptly, one of the 1st story corner columns reached CP level after the 1st peak of the velocity pulse ($t = 6.2$ s).
LCN	Three columns of the 1st story reached CP level at $t = 10.8$ s after the 1st peak of the velocity pulse.
JOS	No structural damage occurred.

It is clear from Figure 17 that a near-fault spectrum has a narrow velocity-sensitive region compared with a far-fault spectrum. Furthermore, the acceleration-sensitive region extends to higher periods (lower frequencies). The latter statement means that the strength demand is more significant than the ductility demand for designing mid-rise buildings as well as low-rise ones in the near-fault zone.

Earthquake-induced force may be reduced due to the ductility provided for structural members. The ductility-dependent component of response modification factor, named ductility reduction factor (R_μ), presents this reduction. The R_μ demand of a ground motion may be defined as the ratio of the elastic spectral acceleration to the inelastic spectral acceleration. In this study, elastic and inelastic spectra are founded by using seismosignal software. Moreover, elastic-plastic SDoF systems with 5% strain-hardening ratio and different ductilities are assumed for deriving the inelastic spectra. Figures 18 and 19 demonstrate the influence of ductility enhancement on the R_μ demand for two instances of the far-fault earthquakes, while Figures 20 and 21 are associated with the near-fault earthquakes. Comparison of R_μ demand indicates the negligible effect of ductility enhancement on the R_μ of near-fault records, especially for transversal component of earthquakes, including forward-directivity effects. Tables 10 and 11 include the R_μ demand associated with the fundamental periods of studied buildings.

As a consequence, enhancing ductility of structures does not considerably change the R_μ demand of near-fault ground motions for structures whose first periods are lower than 1 s or sometimes 1.5 s. On the other hand, the R_μ demand of a far-fault

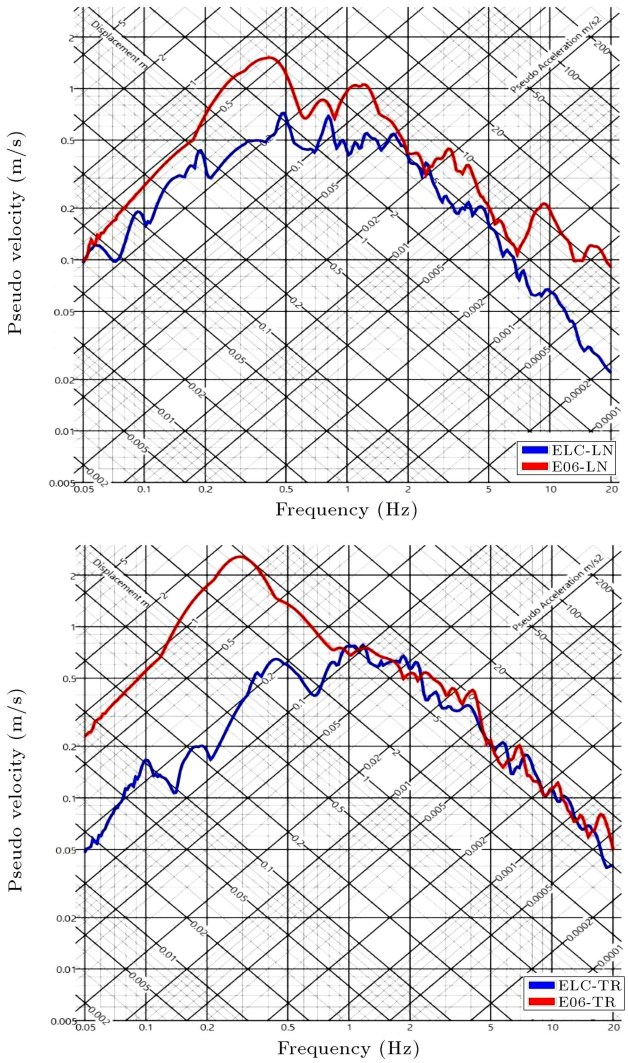

Figure 17. Tripartite spectra of far-fault (ELC) and near-fault (E06) earthquakes.

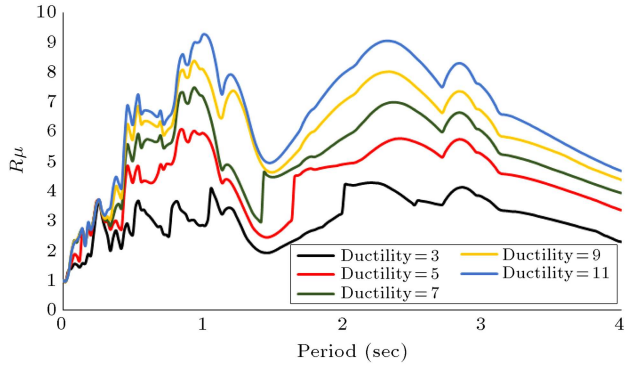

Figure 18. R_μ demand of ELC-TR.

earthquake as well as a weak near-fault earthquake can be increased by enhancing ductility. The results of records such as ERZ, WPI, and BAM confirm the aforementioned discussion, as reported in Tables 10 and 11. Accordingly, it is necessary to enhance the

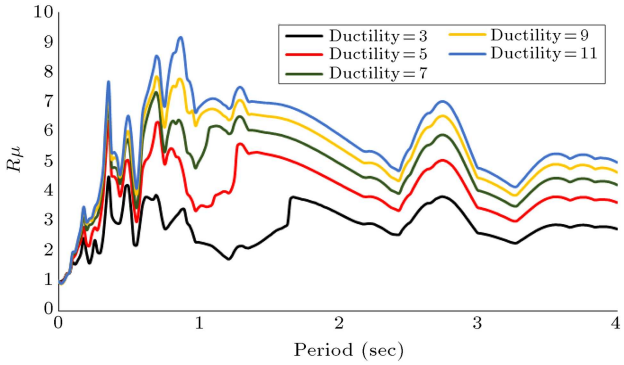

Figure 19. R_μ demand of Taft 1952-LN (far-fault).

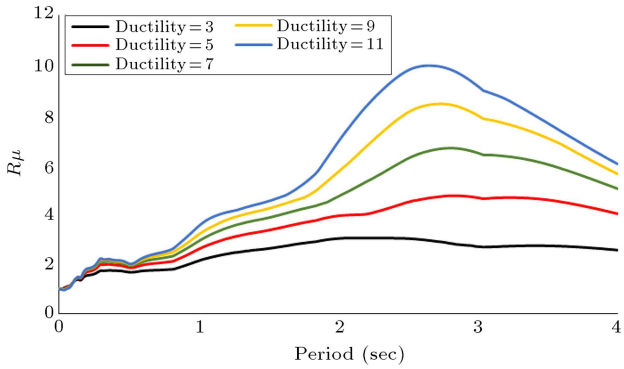

Figure 20. R_μ demand of ERZ-TR.

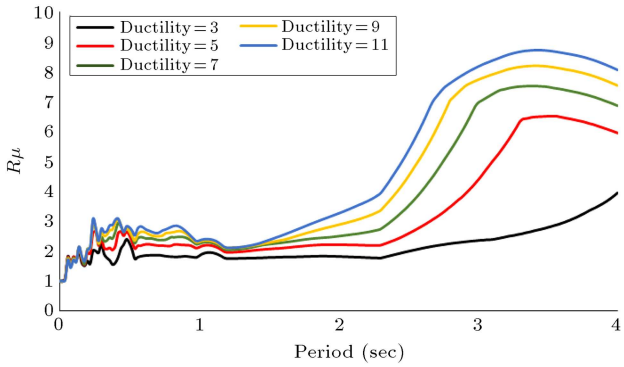

Figure 21. R_μ demand of E06-TR.

strength for improving the performance of the buildings under pulse-type ground motions. In particular, the ductility of the buildings cannot be mobilized ideally due to the high-amplitude pulses of the near-source earthquakes and, therefore, local brittle failures occur.

5. Conclusions

Structures located close to active faults must be assessed precisely because of the impulsive nature of strong near-fault ground motions. It is important to provide desirable strength of structural components so as to avoid the brittle failures, especially at columns. In the present paper, 4 issues were studied. The issues were associated with the scaling of accelerograms,

Table 10. R_μ demand of earthquakes associated with fundamental period of 5-story building.

		R_μ for 5-story building				
No.	**Component**	**Ductility=3**	**Ductility=5**	**Ductility=7**	**Ductility=9**	**Ductility=11**
1	ELC-LN	2.51	3.79	4.35	4.84	5.11
2	ELC-TR	2.80	4.58	5.68	6.16	6.50
3	ABR-LN	3.85	5.69	6.96	7.71	8.11
4	ABR-TR	1.87	2.69	3.20	3.31	3.40
5	SPV-LN	1.65	5.52	6.29	6.67	6.95
6	SPV-TR	2.63	3.27	3.71	4.29	4.82
7	WPI-LN	1.93	2.44	2.76	3.02	3.24
8	WPI-TR	1.53	1.65	1.71	1.76	1.78
9	ERZ-LN	2.93	3.52	3.92	4.29	4.95
10	ERZ-TR	1.74	2.01	2.18	2.30	2.39
11	BAM-LN	2.54	2.77	2.86	2.88	2.93
12	BAM-TR	1.87	2.15	2.33	2.43	2.50
13	TAB-LN	2.22	3.90	4.21	4.48	4.72
14	TAB-TR	2.72	3.62	4.26	4.65	4.91
15	E06-LN	2.51	3.62	3.96	4.11	4.11
16	E06-TR	1.86	2.20	2.40	2.51	2.61
17	E07-LN	3.08	4.06	4.74	5.14	5.50
18	E07-TR	2.52	3.20	3.66	4.00	4.25
19	LCN-LN	2.82	3.93	4.87	5.27	5.50
20	LCN-TR	1.87	2.34	2.60	2.81	2.93
21	JOS-LN	3.62	5.33	6.43	7.21	7.76
22	JOS-TR	3.41	4.76	5.83	6.60	7.05
23	Taft-LN	3.75	5.74	7.15	7.44	8.11

Table 11. R_μ demand of earthquakes associated with fundamental period of 10-story building.

		R_μ for 10-story building				
No.	**Component**	**Ductility=3**	**Ductility=5**	**Ductility=7**	**Ductility=9**	**Ductility=11**
1	ELC-LN	2.66	3.24	3.36	3.95	4.40
2	ELC-TR	3.90	5.33	6.01	7.21	8.62
3	ABR-LN	1.81	2.55	3.70	4.04	4.14
4	ABR-TR	3.28	3.75	4.01	4.76	5.85
5	SPV-LN	2.15	3.38	4.27	5.09	5.78
6	SPV-TR	2.25	3.43	5.20	6.98	8.53
7	WPI-LN	2.15	3.29	4.70	4.83	4.93
8	WPI-TR	1.99	2.43	2.72	2.96	3.16
9	ERZ-LN	1.87	3.32	4.31	4.54	4.81
10	ERZ-TR	2.25	2.78	3.15	3.44	3.82
11	BAM-LN	2.18	3.46	4.51	5.54	6.28
12	BAM-TR	2.60	3.16	3.53	3.81	4.03
13	TAB-LN	2.07	2.30	2.50	2.74	2.98
14	TAB-TR	2.26	2.54	2.81	2.98	3.08
15	E06-LN	2.55	3.28	3.62	3.69	3.72
16	E06-TR	1.95	2.19	2.29	2.35	2.40
17	E07-LN	2.32	5.58	6.98	7.57	8.05
18	E07-TR	1.94	2.47	2.82	3.14	3.38
19	LCN-LN	3.66	5.04	5.46	5.51	5.71
20	LCN-TR	1.79	2.18	2.43	2.61	2.75
21	JOS-LN	2.69	3.99	5.37	6.76	7.85
22	JOS-TR	4.06	4.87	5.48	6.22	7.50
23	Taft-LN	2.22	3.52	6.13	6.77	7.11

the demands in LRHA and NRHA, the vulnerable members, and the effect of ductility enhancement. The following conclusions were attained after assessing the mid-rise RC moment frame buildings under near-fault earthquakes.

1. The design spectrum of Iranian seismic code (IS 2800-14) is not compatible with spectra of near-fault records having forward-directivity effects, especially for longer periods, and this problem leads to insufficient demand. Furthermore, it is appropriate to use the single scaling method instead of the average scaling method for avoiding the attenuation of the peaks existing in the near-fault spectra. It could be more desirable to employ a specific spectrum of near-fault earthquakes in the design;
2. Implementation of LRHA using response modification factor (R_u) and deflection amplification factor (C_d) yields inaccurate values of inter-story drift ratio for seismic assessment. Implementation of NRHA is more reasonable in order to specify the accurate inter-story drift ratio as well as the accurate design base shear;
3. Damages to the 10-story building are more than those to the 5-story building. The most vulnerable members of moment frames are the first story corner columns attacked severely at such a time close to the pulse peak or at the end of the pulse;
4. Enhancing the ductility, especially for periods shorter than 1 or 1.5 s, does not make considerable changes in the R_μ demand of the strong near-fault earthquakes. It seems that strength enhancement could be more efficient than ductility enhancement and significant care should be taken of the strength as the most noteworthy concern for designing in near-fault zones.

Acknowledgements

The researchers dedicate this research to the people who lost their lives and properties in near-fault earthquakes such as Tabas 1978 and Bam 2003.

References

1. Stewart, J.P., Chiou, S.J., Bray, J.D., Graves, R.W., Somerville, P.G., and Abrahamson, N.A. "Ground motion evaluation procedures for performance-based design", *Soil Dyn. And Earthq. Engrg.*, **22**(9), pp. 765-772 (2002).
2. Alavi, B. and Krawinkler, H. *Effects of Near-fault Ground Motions on Frame Structures*, John A. Blume Earthq. Engrg. Center, California, USA (2001).
3. Bolt, B.A. "The San Fernando earthquake, 1971. Magnitudes, aftershocks, and fault dynamics", *Bull.*, 196 (1975).
4. Anderson, J.C. and Bertero, V.V. "Uncertainties in establishing design earthquakes", *J. of Struct. Engrg.*, **113**(8), pp. 1709-1724 (1987).
5. Kalkan, E. and Kunnath, S.K. "Effects of fling step and forward-directivity on seismic response of buildings", *Earthq. Spect.*, **22**(2), pp. 367-390 (2006).
6. Chang, T.P. and Yu, G.K. "A study of strong motion response spectrum in west-central Taiwan", *Terrestrial, Atmospheric and Oceanic Sciences.*, **13**(2), pp. 135-152 (2002).
7. Choi, I., Kim, M.K., Choun, Y.S., and Seo, J.M. "Shaking table test of steel frame structures subjected to scenario earthquakes", *Nuclear Engrg. And Tech.*, **37**(2), pp. 191-200 (2005).
8. Choi, H., Saiidi, M.S., Somerville, P., and El-Azazi, S. "Bridge seismic analysis procedure to address near-fault effects", *A Report of Nevada University* (Reno), Virginia, USA (2005).
9. Su, F., Anderson, J.G., and Zeng, Y. "Characteristics of ground motion response spectra from recent large earthquakes and their comparison with IEEE standard 693", In *Proceed. of 100th Anniv. Earthq. Conf., Commemorating the 1906*, pp. 18-22 (2006).
10. Hatzigeorgiou, G.D. "Ductility demand spectra for multiple near-and far-fault earthquakes", *Soil Dyn. And Earthq. Engrg.*, **30**(4), pp. 170-183 (2010).
11. Durucan, C. and Durucan. A.R., "A p/V p specific inelastic displacement ratio for the seismic response estimation of SDOF structures subjected to sequential near fault pulse type ground motion records", *Soil Dyn. And Earthq. Engrg.*, **89**, pp. 163-170 (2016).
12. Yaghmaei-Sabegh, S. and Tsang, H.H. "An updated study on near-fault ground motions of the 1978 Tabas, Iran, earthquake (Mw= 7.4)", *Scientia Iranica*, **18**(4), pp. 895-905 (2011).
13. Champion, C. and Liel, A. "The effect of near-fault directivity on building seismic collapse risk", *Earthq. Engrg. And Struct. Dyn.*, **41**(10), pp. 1391-1409 (2012).
14. Alavi, B. and Krawinkler, H. "Strengthening of moment-resisting frame structures against near-fault ground motion effects", *Earthq. Eng. And Struct. Dyn.*, **33**(6), pp. 707-722 (2004).
15. Massumi, A., Mahboubi, B., and Ameri, M.R. "Seismic response of RC frame structures strengthened by reinforced masonry infill panels", *Earthq. And Struct.*, **8**(6), pp. 1435-1452 (2015).
16. Mortezaei, A., Ronagh, H.R., and Kheyroddin, A. "Seismic evaluation of FRP strengthened RC buildings subjected to near-fault ground motions having fling step", *Compos. Struct.*, **92**(5), pp. 1200-1211 (2010).
17. Ponzo, F.C., Di Cesare, A., Nigro, D., Vulcano, A., Mazza, F., Dolce, M., and Moroni, C. "JET-PACS project: Dynamic experimental tests and numerical results obtained for a steel frame equipped with hysteretic damped chevron braces", *J. of Earthq. Engrg.*, **16**(5), pp. 662-685 (2012).

18. Mazza, F. "Nonlinear incremental analysis of fire-damaged r.c. base-isolated structures subjected to near-fault ground motions", *Soil Dyn. and Earthq. Engrg.*, **77**, pp. 192-202 (2015).

19. Mazza, F. "Nonlinear response of r.c. framed buildings retrofitted by different base-isolation systems under horizontal and vertical components of near-fault earthquakes", *Earthq. And Struct.*, **12**(1), pp. 135-144 (2017).

20. Sorace, S. and Terenzi, G. "A viable base isolation strategy for the advanced seismic retrofit of an R/C building", *Contemp. Engrg. Sci.*, **7**(17-20), pp. 817-834 (2014).

21. Mazza, F. "Comparative study of the seismic response of RC framed buildings retrofitted using modern techniques", *Earthq. And Struct.*, **9**(1), pp. 29-48 (2015).

22. Grigorian, C.E. and Grigorian, M. "Performance control and efficient design of rocking-wall moment frames", *J. of Struct. Engrg.*, **142**(2), 04015139 (2015).

23. Rahgozar, N., Moghadam, A.S., and Aziminejad, A. "Inelastic displacement ratios of fully self-centering controlled rocking systems subjected to near-source pulse-like ground motions", *Engrg. Struct.*, **108**, pp. 113-133 (2016).

24. Gerami, M. and Abdollahzadeh, D. "Estimation of forward directivity effect on design spectra in near field of fault", *J. of Basic. and app. Scifc. Res.*, **2**(9), pp. 8670-8686 (2012).

25. American Concrete Institute, *Building Code Requirements for Structural Concrete (ACI 318-14)*, Michigan, USA (2014).

26. *Iranian Code of Practice for Seismic Resistant Design of Building, Standard No. 2800* (4th Edition), Tehran, Iran (2014).

27. American Society of Civil Engineers (ASCE), *Minimum Design Loads for Buildings and Other Structures (ASCE/SEI 7-10)*, Virginia, USA (2010).

28. Haselton, C.B., Whittaker A.S., Hortacsu A., Baker J.W., Bray J., and Grant D.N. "Selecting and scaling earthquake ground motions for performing response-history analyses", In *Proceed. of the 15th World Conf. on Earthq. Engrg.* (2012).

29. American Society of Civil Engineers (ASCE), *Seismic Evaluation and Retrofit of Existing Buildings (ASCE/SEI 41-13)*, Virginia, USA (2013).

30. Takeda, T., Sozen, M.A., and Nielsen, N.N. "Reinforced concrete response to simulated earthquakes", *J. of the Struct. Dyn.*, **96**(12), pp. 2557-2573 (1970).

31. Hilber, H.M., Hughes, T.J., and Taylor, R.L. "Improved numerical dissipation for time integration algorithms in structural dynamics", *Earthq. Engrg. And. Struct. Dyn.*, **5**(3), pp. 283-292 (1977).

32. Sehhati, R., Rodriguez-Marek, A., ElGawady, M., and Cofer, W.F. "Effects of near-fault ground motions and equivalent pulses on multi-story structures", *Engrg. Struct.*, **33**(3), pp. 767-779 (2011).

33. Tasnimi, A.A. and Massumi, A., *Estimation of Response Modification Factors for RC-MRF Structures*, Building and Housing Research Center (BHRC), Tehran, Iran (2007).

Biographies

Mohammad Hossain Mohammadi is a researcher in Tehran, Iran. He holds BSc degree, received in 2013, in Civil Engineering from Shahid Rajaee University and MSc degree, received in 2016, in Structural Earthquake Engineering from Kharazmi University as the first top student. His research interest is in seismic design and assessment of structures, concentrating on pulse-type excitations.

Ali Massumi received his PhD from Tarbiat Modares University in 2004. He is a full Professor in Structural and Earthquake Engineering at Kharazmi University. He has been a visiting researcher at the University of Ottawa, Canada, in 2003, and a visiting scholar at the University of California, Los Angeles (UCLA), in 2013. His research activities mainly deal with structural and earthquake engineering including seismic behavior of RC structures, damage detection and assessment, seismic soil-structure interaction, progressive collapse, and retrofitting. He is author or co-author of 12 books, technical regulations, and technical reports. He has published more than 100 papers in refereed journals and conferences.

Afshin Meshkat-Dini is an Assistant Professor at Kharazmi University. He received his PhD in Structural Engineering from Amirkabir University of Technology. He has published a variety of structural engineering papers, specifically on seismic performance of high-rise buildings in near-fault zones. Now, he teaches and researches on seismic design of tall buildings, finite element method, and strong near-source pulse-type ground motions.